Journal of Manufacturing Processes 56 (2020) 1322–1330

Contents lists available at ScienceDirect

Journal of Manufacturing Processes

journal homepage: www.elsevier.com/locate/manpro

A numerically controlled shape memory alloy wire bending process using vat photopolymerization

Han Xu[a], Shuai Chen[b], Fuyuan Luo[c], Huachao Mao[d], Yong Chen[a,b,*]

[a] Epstein Department of Industrial and Systems Engineering, University of Southern California, Los Angeles, CA, USA
[b] Department of Aerospace and Mechanical Engineering, University of Southern California, Los Angeles, CA, USA
[c] Department of Mechatronics Engineering, Nanjing University of Aeronautics and Astronautics, Nanjing, China
[d] School of Engineering Technology, Purdue University, West Lafeyette, IN, USA

ARTICLE INFO

Keywords:
Wire bending
Numerical control
Vat photopolymerization
Shape memory alloy

ABSTRACT

The fabrication of shape memory alloy (SMA) based products requires the precise bending and high-temperature training of SMA wires to obtain desired two-dimensional (2D) and three-dimensional (3D) patterns. In the typical fabrication process, SMA wire is bent and fixed in a pre-built mold and is trained using a furnace. However, in the small batch production, the fabrication of a mold that can be put in a high-temperature oven is costly and requires a long time to fabricate. A novel SMA wire bending process using vat photopolymerization (VPP) is presented in this paper. A rotary wire extruding system was designed to control the feeding speed of the fed wire and the bending of the wire into the desired shape. The wire bending process was enabled by utilizing a VPP tool that was immersed in liquid resin to selectively cure the resin to firmly fix the extruded SMA wire on a substrate. An air bubble assisted separation process was developed to address the separation of the cured resin from the immersed VPP tool. After the bending of the SMA wire into the desired shape, the SMA wire was connected to an electric current to heat the wire to a high temperature required by the training process so the SMA wire can memorize the fabricated pattern. Finally, the photocured fixtures deposited by the VPP tool were dissolved by a chemical solution and the bent SMA wire was detached from the fixture that was ready to use. The developed numerically controlled wire bending process is flexible for designed patterns and can fabricate SMA wires into 2D/3D shapes without specific molds or tedious manual work. Several test cases were performed to demonstrate the effectiveness of the newly developed SMA wire bending process.

1. Introduction

Shape memory alloys (SMA) were first invented by Arne Ölander in 1932 [1], which possess shape memory and superelastic effects. The shape memory effect reverses the SMAs under plastic deformation and restores the undeformed shape in a raised temperature. The superelastic effect (also called pseudo-elasticity effect) reverses the SMAs to undeformed shape after the removal of a relatively high external strain at a low temperature. This unique property is due to the changes in the crystallographic structure depending on the temperature. At a low temperature, the SMAs will be in the martensite state where SMAs are easy to be deformed. While in a raised temperature, the SMAs return into a uniform austenite state, which has the same macroscope shape as the pre-deformed shape.

The shape memory effect and the superelastic effect provide lots of engineering opportunities for SMA wires in various fields, including automotive, aerospace, robotic and biomedical industries. For example, in the automobile industry, the demands of comfort, efficiency, and safety increase the use of “smart” components such as micro-actuators, and sensors used in vehicles. The SMAs actuators, due to their lightweight and small size properties, provided better performance on vehicles compared with conventional actuators [2]. It was reported that the fuel door actuator made from SMA wire was 70 % lighter than the conventional direct current (DC) actuator. The rear-view mirror folding, the climate control flaps adjustment, and the lock and latch controls have all taken advantage of shape memory alloys [3,4].

Similarly, in the aerospace industry, SMA couplings were used on the plane due to the properties such as high dynamic load and geometric shape constrain [5]. Other aerospace components such as structural connectors, vibration dampers, sealers, release or deployment mechanisms, inflatable structure, manipulators, and pathfinder applications also took advantage of shape memory alloys [6,7]. In the

* Corresponding author at: Epstein Department of Industrial and Systems Engineering, University of Southern California, Los Angeles, CA, USA.
E-mail address: yongchen@usc.edu (Y. Chen).

https://doi.org/10.1016/j.jmapro.2020.04.027
Received 2 December 2019; Received in revised form 1 March 2020; Accepted 11 March 2020
Available online 17 June 2020

robotic field, shape memory alloys were first used as micro-actuators or electric muscles in the 1980s [8]. In recent years, the traditional robot components such as robotic joint, gripper, micro-wheel, and bio-mimic finger were designed using the SMA actuator [8–10,13]. In the biomedical industry, SMAs were widely used in biomedical devices including teeth braces, endodontics, stents, medical tweezers, sutures, and anchors due to their high corrosion resistance and biocompatibility [10–12].

A large portion of the devices mentioned above were fabricated from SMA wires. For example, the SMA actuators such as a bio-mimic finger, linear actuator, electronic muscle, and the SMA fixtures, including teeth braces and heart stents, were all bent or reshaped from SMA wires. However, there is a lack of high precision and fast manufacturing process to shape and train SMA wires.

1.1. Traditional SMA wire bending process

Given the demands of SMA in industrial fields, several fabrication processes have been developed. Most of the SMA-wire-based devices use simple shapes such as spring shape or straight line as actuators mainly because of easy fabrication. Actuators in these simple shapes can be fabricated by a molding process, in which the SMA is bent and fixed into a pre-built mold, and a raised temperature is applied for SMA to memorize the formed shape. However, the molding approach significantly restricts the design freedom, so the SMA wires can only have simple and mostly one-dimensional (1D) shapes. For the SMA products with more complex shapes such as dental teeth braces and vessel stents, people usually have to rely on manual works, which is time-consuming with low accuracy.

To make use of the intrinsic multi-directional actuating capability of SMA, a few efforts have been made to investigate the bending and training process of a SMA wire to form complex three-dimensional (3D) shapes. Kaori Kuribayashi developed a self-deployable origami SMA stent with a folding method [14,15]. A laser machining process of the SMA tubing catheter was invented by Tung et al. [16]. Also, a sophisticated robot to bend SMA braces was developed by Gilbert [17]. The use of a bending robot increased the fabrication speed and accuracy. However, it can only provide the first order bending, while the other two dimensional bending needs to be accommodated with the standard bending process. Rodrigue, et al. used PDMS as a soft mold to fabricate SMA with complex geometric shapes [18]. A double molding technique was used to fabricate low stiffness SMA wires into multiple curved features. More recently, Elwany et al. investigated the use of the selective laser sintering process to directly fabricate SMA wires with location-specific properties [19].

1.2. Contributions

Although many efforts have been made previously, the numerically controlled bending of SMA wires into complex 2D/3D patterns is still expensive and time-consuming. One key challenge is, compared to the conventional metal wire bending process, the SMA wire bending requires a mold as the fixture of the wire during the high-temperature training process [20]. Otherwise, the SMA wire will bounce back during the heat training process because of the shape memory effect. However, the fabrication of the mold significantly increases the cost and decreases the fabrication speed.

In this paper, we present a mold-free and numerical controlled SMA wire bending process by integrating one of the additive manufacturing (AM) processes, vat photopolymerization (VPP), during the wire bending process. We used VPP to dynamically build a set of polymer-based fixtures to enable the bending the SMA wire using a numerically controlled bender. Consequently, a spool of SMA wire can be bent into a designed pattern that was digitally defined in a computer aided design (CAD) system. The hardware and software systems of the VPP-based SMA wire bender are presented in the paper. A critical issue on reducing the separation force between the VPP tool and the photocured fixtures during the wire bending process was solved using an air bubble as the curing interface of the VPP tool. We performed several designed test cases to verify the developed wire bending process. The fabrication quality of the wire bending results was analyzed to understand the precision of the developed wire bending process.

The remainder of the paper is organized as follows. Section 2 discusses the recent research related to this work. Section 3 discusses the principle of the SMA wire bending process. Section 4 demonstrates the hardware and software systems to that have been developed realize the desired wire bending results. Section 5 investigates the air bubble assisted separation method to achieve strong fixture of the SMA wire and to reduce the separation force between the photocured fixtures and the VPP tool. Section 6 discusses the SMA training and fixture removal processes. Section 7 presents several test cases to demonstrate the capability of the numerically controlled wire bending process. Finally, Section 8 concludes the paper with future work.

2. Related works

The vat photopolymerization process is one of the most widely used AM processes. The original stereolithography apparatus (SLA) was invented by Charles Hull in the 1980s. The SLA process can fabricate 3D models by selectively converting liquid photocurable resin into solid using a controlled ultraviolet (UV) laser. When exposed to UV light, the photoinitiator mixed in the liquid resin will trigger the photopolymerization process of the liquid resin to form solid polymer. A bottom-up-based SLA process will constrain the liquid resin into 100 microns layers by controlling the gap between the printed layers and the resin tank. In addition to the galvanometer-mirror-based laser, more VPP systems nowadays use a digital micromirror device (DMD) with a light source to selectively solidify a thin layer of liquid resin into desired 2D patterns.

In recent years, efforts on developing non-layer-based VPP processes to achieve multi-material, multi-scale, and multi-function fabrication capability have been made. In our previous work, Chen et al. developed a layerless additive manufacturing process named CNC accumulation [21]. In the CNC accumulation process, an optical fiber was used to directly send UV energy to a spot inside the liquid resin. Hence, by controlling the on/off state of the UV-LED and the multi-axis motion of the optical fiber, a physical model can be built by selectively curing liquid resin into solid by following a planned toolpath. Based on the idea, Pan et al. developed a set of optical fiber tools with various sizes and shapes [22]. The additional accumulation tools increased the accumulation speed and shape complexity of CNC accumulation. Recently, an immersion-based stereolithography process called linear immersed sweeping accumulation (LISA) was developed by Mao et al. [23]. LISA utilized an immersed linear accumulation tool using a galvanometer-mirror-controlled laser to fabricate 3D shapes line by line. The resin will be exposed to a moving line pattern during the solidification process. Hence the LISA process is much faster than the point-based CNC accumulation method. Li and Chen [24] further developed a surface-based CNC accumulation process using a DMD, which can achieve a good balance between fabrication speed, feature resolution, and shape flexibility.

Based on the previous study of the CNC accumulation processes, this paper presents a numerical controlled wire bending process that uses an immersed VPP tool to selectively cure liquid resin into solid fixtures. Consequently, the dynamically built fixtures can be used to facilitate the wire bending process as well as the SMA wire training process.

3. VPP-based wire bending process

The VPP-based SMA wire bending process is shown in Fig. 1. Firstly, An input computer-aided design (CAD) model of a wire pattern is converted into the tool path for the VPP-based wire bending system.

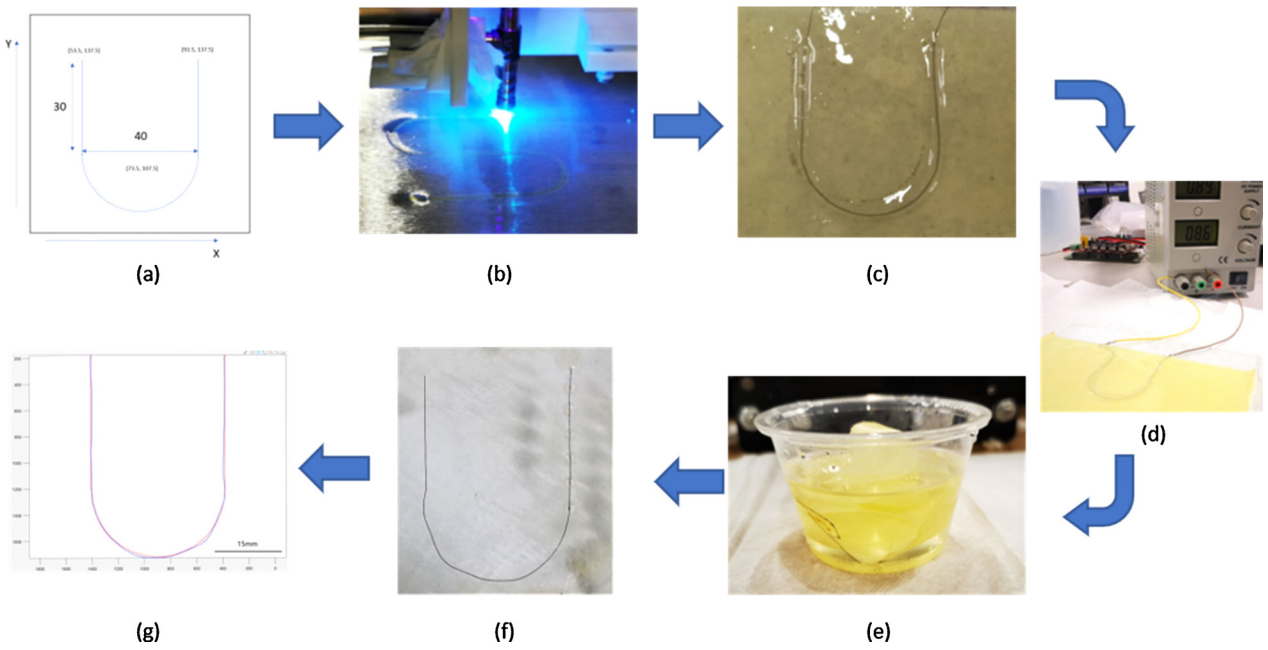

Fig. 1. Workflow of the wire bending process. (a) Digital design of a wire bending pattern; (b) numerically controlled wire bending; (c) bent SMA wire with dynamically cured polymer fixtures; (d) heat training of the SMA wire; (e) polymer fixture dissolving in the chemical solution; (f) automatic shape recovery of the trained SMA wire in a raised temperature; and (g) error analysis result after the shape recovery.

Then, based on the tool path, a SMA wire is bent dynamically using the cured fixtures, which are fabricated on the substrate by the immersed VPP accumulation tool in liquid resin. The cured liquid resin embeds and fixes the bent SMA wire into the desired pattern on the substrate. The fixed positions of the SMA wire are numerically controlled by a 4-axis moving platform. The bending of the SMA wire is facilitated by the designed fixtures that are dynamically cured during the wire bending process. After the wire has been bent into the designed pattern, the SMA wire and the substrate will be taken out of the resin tank. The SMA wire is then applied with 1.6 Amps current to raise its temperature over 500 °C to train the wire. After the SMA training process, the programmed shape pattern was memorized by the SMA wire. Consequently, the polymer fixtures can then be dissolved using a chemical solution or by manual work at the room temperature. The trained SMA wire now can be deformed to any shape but it will quickly return to the initially trained shape when the wire is exposed to a raised temperature.

Fig. 2 shows the schematic illustration of a SMA wire bending process, including the wire bending unit and an immersed VPP tool related to the SMA wire. The wire bending unit extrudes and twists the SMA wire so the wire can be deformed into the designed shape defined by the CAD model. The immersed VPP tool builds solidified fixtures using the liquid photocurable resin to facilitate the bending of the SMA wire and to maintain its shape during the SMA wire training process with a raised temperature over 500 °C.

The wire extruding system is designed to feed, bend, and deposit the SMA wire from a spool into any controlled positions over time. A wire extruder guides a spool of SMA wire to a planned position, where a UV laser shoots a focused spot to fix the wire on the substrate. The fed SMA wire will be bend by a wire extruder nozzle into the designed shape and fixed by photocured resin onto the substrate. In order to bend the wire into any curved shape, the wire extruder was mounted on a rotary stage to extrude the SMA wire in 360 degrees on the surface of the substrate. Both the wire extruder and the laser guiding tube are mounted on a *XYZ* liner stage. By numerically control the linear movement of the wire extruder and the laser dot as well as the rotation of the wire extruder, the shape of the bent SMA wire can be digitally controlled by fixing it on the bottom substrate (see Fig. 3).

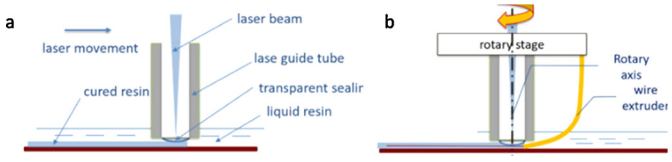

Fig. 2. An illustration of the SMA wire bending process. (a) The immersed VPP process to dynamically cure fixtures for the bent wire; and (b) the wire bending process using the immersed VPP tool.

The immersed VPP tool provides a UV laser beam on the bent SMA wire, which is submerged inside the liquid photocurable resin. The liquid resin surrounding the SMA wire will be solidified after the exposure to the UV laser beam. Hence the solidified resin will fixe the SMA wire firmly on the substrate. With the aid of the fixture, the SMA wire can now be continuously bent into a target shape. Different from the layer-based SLA that also uses a laser, the immersed VPP tool has a metal tube to guide the laser energy inside liquid resin to selectively cure the resin around the wire so that the SMA wire can be accurately bent into a desired shape.

Some other design considerations for using the immersed VPP tool to fix the SMA wire during the wire bending process include the following considerations. (1) The solidified resin needs to have sufficient Young's modulus (e.g., the resin we used from Formlabs has Young's Modulus of 1.6 GPa [20]). Compared to PDMS (1.36 MPa, 10:1 PDMS) [21], the photocured polymer can better serve as the wire fixture that will not change its shape under the external bending force. (2) The immersed VPP tool can cure resin on both a flat surface and a curved surface. The fixture fabrication on a curved surface requires one to pre-fabricate a 3D substrate that has the designed curved surface to fix SMA wire into 3D shape. As shown in our previous work, photocured fixtures can be fabricated on a curved substrate using the build-around-insert capability enabled by the five-axis computer numerical controlled (CNC) accumulation process [22–26]. Consequently, a SMA wire can be bent on the curved surface during the wire bending process to enable the bending of the SMA wire into a 3D curved pattern.

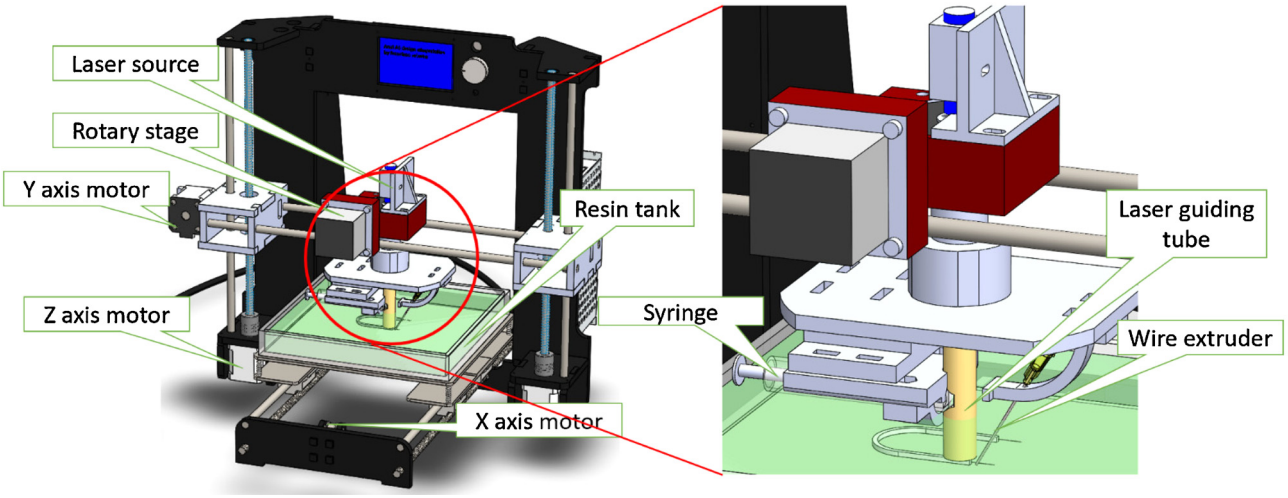

Fig. 3. The SMA wire bending system design.

4. Hardware and software design

A prototype system has been developed to verify the VPP-based SMA wire bending process. The main hardware and software systems were designed with a 4-axis linear system, a rotation stage, and an immersed VPP tool.

4.1. Hardware design

A 3-axis *XYZ* linear stage was used to control the position of the immersed VPP tool and the wire extruder (see Fig. 3-left). The immersed VPP tool included a 405 nm UV laser diode (0.27 W), a laser guide tube whose diameter was 10 mm, a 5 mL syringe to control the air bubble formed on the tip, and a rotary stage that was mounted on the *XYZ* linear stage (see Fig. 3-right). The laser diode shot a laser beam whose diameter was controlled to be around 0.5 mm. The laser diode can be dynamically turned on and off. When the UV laser was turned on, the laser power was controlled to be 270 mW. The laser beam passed through the center of the laser guide tube, and when it was turned on all the liquid resin under the laser beam would be cured. The air bubble controlling syringe was connected to the laser guide tube to control the air pressure inside the tube so that positive air pressure was maintained to form an air bubble that prevented liquid resin from flowing inside the tube. The rotation stage was mounted collinearly with the center of the laser guide tube so that the rotation of the wire bending tool only changed the direction of the wire extruder. The wire extruder had a nozzle whose diameter was 0.8 mm to allow any SMA wires with smaller diameter sizes to pass through. The wire extruder has the four-axis motion control capability including a 3-xis linear stage and a rotary stage. A 200 mm × 200 mm glass resin tank with a removable building platform was used as the test substrate for the SMA wire bending system. The SMA wire used in the bending test had the diameter of 150 microns (purchased from Flexinol Inc.). The controller was an Arduino mega 2560 board, which integrated the control board and the driver board to control the 4-axis motion. The software used in the control board was the Marlin open-source 3D printing firmware. Table 1 lists the main components used in the SMA wire bending system.

The distance between the wire extruder and the laser spot needs to be controlled to prevent the nozzle used in the wire extruder from clogging. That is, the substrate may reflect the light of the laser spot and the reflected light can be absorbed by the surrounding resin. Usually, the reflected laser energy is weak and will not be able to cure liquid resin in a short time. However, if the resin around the nozzle of the wire extruder is continuously exposed to the reflected laser light during the entire fabrication process, the accumulated energy may still be able to cure some resin on the tip of the nozzle, which will block the wire extruder. The minimum distance between the laser spot and the wire extruder would depend on the laser beam size and the laser energy as well as the light reflection property of the substrate. For a bigger laser spot size and higher laser energy, a larger distance is required to avoid the clogging of the wire extruder. In our experiment, the minimum gap between the nozzle and the laser spot d_{min} was set at 5 mm for the laser power $P =$ 270 mW, laser spot size $d = 500\,\mu m$, and the laser guide tube size $d_n = 10$ mm. The same parameters were used in all the test cases.

Table 1
Main components of the wire bending system.

Component	Parameter	Description
Laser	λ = 405 nm	Wavelength
	P = 0–270 mW	Power
	dl = 500 μm	Diameter
Wire extruder	de = 0.8 mm	Diameter
Rotary stage	res = 0.01°	
Syringe	v = 5 mL	
SMA wire	dw = 150 μm	Flexinol

4.2. Software design

The wire bending software system controls the moving path of the UV laser beam, the rotation angle of the wire extruder, and the laser on/off status. The software was designed based on the laser-based CNC accumulation process [21]. The tool path of a straight line was the same as the laser-based CNC accumulation tool path. However, since an additional rotation stage was added to the setup, the tool path of a curved line was converted into a polygonal chain first (see Fig. 4). A curve was divided into several small line segments with equal central angle θ.

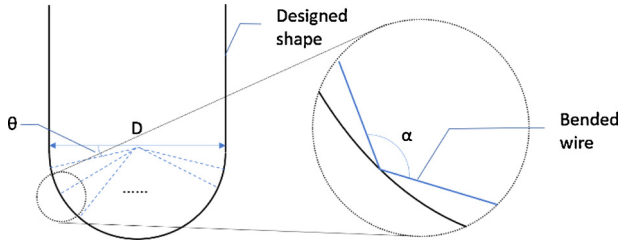

Fig. 4. An illustration of the wire bending tool path.

Table 2
A G-code example.

Line	G-code	Description
N010	L0	Initialization of laser
N020	G29	Tool homing
N030	G01 Z190 F100	Move Z stage
N040	G01 X50 Y60 F100	Move X, Y stages
N050	L80	Turn on laser
N060	G01 X80 F100	
…	…	…
N200	G01 H161.1 F500	Rotate stage
N210	G01 X84.5 Y89.2 F100	
N220	G01 H179.0 F500	
N230	G01 X79.9 Y89.9 F100	
…	…	…
N500	L0	Laser off
N510	G29	Tool homing

Accordingly, the polygonal tool path was created by connecting the chord of each small segment. Then the rotation angle α between each cord can be obtained as α = (180-θ). By decreasing the central angle of each line segment, the polygonal chain would become a close approximation of the given curve. Consequently, we can achieve relatively robust and accurate wire bending results.

The VPP-based wire bending tool path was encoded by modifying the standard G-code used in the fused deposition modeling (FDM) 3D printers. We added two additional commands to the conventional commands defined in the G-codes as following:

- L: stands for laser on/off state and the used power. The number following "L" indicates the power of the laser, "0" means "off" and "1" means "on".
- H: stands for the rotation axis. The number following "H" indicates the rotation angle in the unit of degree.

The G-code modified for the 4-axis motion stage can now realize the control of both linear *XYZ* position and the rotation, as well as the pulse-width modulation (PWM) control of the laser diode. An example of the G-code is shown in Table 2.

5. Air bubble separation

A key challenge to be addressed in the VPP-based wire bending process is how to detach the cured resin from the immersed VPP tool inside liquid resin. That is, the VPP tool used in the wire bending process is fully immersed inside liquid resin. Hence the tool will have a laser curing tip and the cured resin will naturally stick to the laser tip instead of the bottom substrate. The building process will then fail if the cured resin cannot be detached from the VPP tool and the SMA wire will not be firmly fixed at a desired position on the substrate. Also, the resin surrounding the laser tip may be solidified by the scattered laser beam after a certain time, which will further increase the required separation force to peel off the cured resin from the laser tip. Fig. 5(a) shows the consequence of a failed separation test case for a tip using a Teflon film.

To address the sticking resin issue, a novel air bubble-assisted separation process has been developed in this work, in which the laser energy is directly guided onto the desired region of liquid resin with a minimal detaching force at the same time. Here we used anadditional syringe to push out a stable air bubble at the bottom outlet of the laser guide tube. A higher air pressure we used inside the tube prevented liquid resin from flowing into the laser guide tube. When the laser was on, the laser beam shot through the guide tube on the center of the air bubble. Consequently, the liquid resin under the air bubble was cured and would attach to the substrate since the attaching force to the air bubble is relatively small (see Fig. 5b). The gap between the air bubble and the building substrate should be smaller than the curing depth of the used liquid resin. In our test, the cure depth is around 1.5 mm based on the designed cure depth tests [26]. Accordingly, we controlled the gap $Z = 1$ mm for the laser power $P =$ 80 mW and the moving speed of the VPP tool $v = 1$ mm/s.

The building result of a 25 mm straight line is shown in Fig. 5(c) and (d). The results show that no cured resin sticks on the VPP tool tip because the separation force between the cured resin and the air bubble surface is smaller than the attaching force of the cured resin to the bottom substrate. Hence the cured resin will stick on the bottom substrate with the SMA wire firmly sealed inside the photocured polymer. We also noticed that the starting point of the cured resin had a circular dent while the other part of the resin had a relatively smooth surface. The reason for the dent is because the upper constrain of liquid resin was an air bubble whose interface was defined by the air pressure and the surface tension of the liquid resin [27]. Consequently, the top surface of the cured resin was not flat. However, such a surface defect or inaccuracy of the cured fixtures is not important in our SMA wire bending process since the wire bending precision will not be affected by the shape of the cured fixtures. Actually, after the wire training process, all the polymer fixtures will be removed from the wire. Hence the developed air bubble-assisted VPP tool is appropriate for the SMA wire bending process.

6. SMA wire training and resin removal

The shape memory alloy used in our tests was TiNi alloy from Flexinol Incorporated. The resistance and the pulling force of the wire when heated are given in Table 3 [28]. In this work, the TiNi alloy wire that we used has a diameter of 0.15 mm, and its resistance is 75 Ohms/meter. The pulling forces of the SMA wire when heated is 321 g. The TiNi SMA wire can be trained using a raised temperature of over 500 ℃ so that the martensite structure transforms into austenite [29]. There are plenty of heating methods that can be used to train the SMA wire. The SMA wire training method used in this study was to apply a controlled electric current on the bent SMA wire for a specific time. The heating temperature is governed by the following equation.

$$T_{\max} = 16.383\frac{I}{d} + 3.987(\frac{I}{d})^2 \quad (1)$$

T_{max} is the highest temperature of the SMA wire (℃); I is the applied current (Amp); and d is the diameter size of the SMA wire (mm). In our work $T_{max} = 500$ ℃, $d = 0.15$ mm, and $I = 1.40$ A. The accurate temperature of the SMA wire during the training process was measured by a TG165 spot thermal camera to ensure the SMA fully transform to austenite.

After the SMA wire training, the polymer fixture were dissolved using a chemical solution. Lots of acid etchants can be used to dissolve photocurable resin [30]. We used apiranha solution composed of one volume of 96 % sulfuric acid and one volume of 30 % hydrogen peroxide. The solution is commonly used to clean the residual polymer on silicon wafers. The dissolving temperature was set at 70 ℃. It took over 2 h to dissolve the photocured polymer that was used as the fixture of the SMA wire to the extent that the wire can be manually separated from the fixture. Other combinations of photocurable resins and etching solutions can also be used in the SMA wire bending process.

7. Experimental results

A prototype system has been built for the VPP-based SMA wire bending process. The system was constructed using a desktop 3D printer (*Alunar*) and integrated the wire feeding system, the VPP tool, and the related air bubble control system into the printer (Fig. 6). Both basic and more complex shapes were designed to test the capability of the constructed VPP-based wire bending system. We demonstrated the controlled bending results using both continuous resin fixtures and

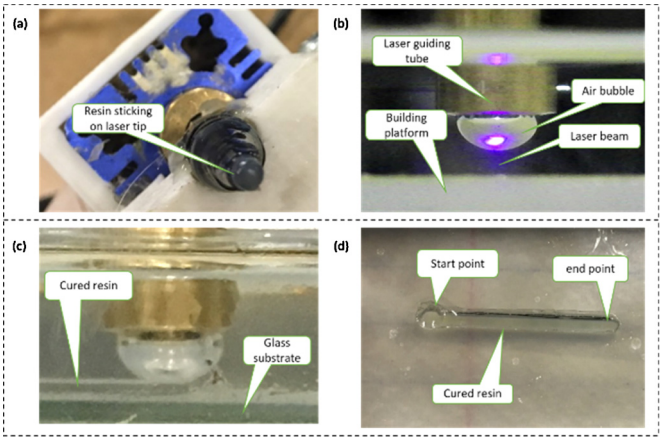

Fig. 5. Air bubble separation. (a) Separation issue of cured resin sticking on the laser tip; (b) the bubble-assisted VPP tool separation; (c) the separation process using an air bubble; and (d) the test result of a fixed line on a flat surface.

Table 3
Flexinol Actuator wire technical data.

Diameter (mm)	Resistance (Ohms/meter)	Pulling force when heated (grams)
0.025	1425	8.9
0.038	890	20
0.050	500	36
0.076	232	80
0.10	126	143
0.15	75	321
0.20	29	570
0.25	18.5	891

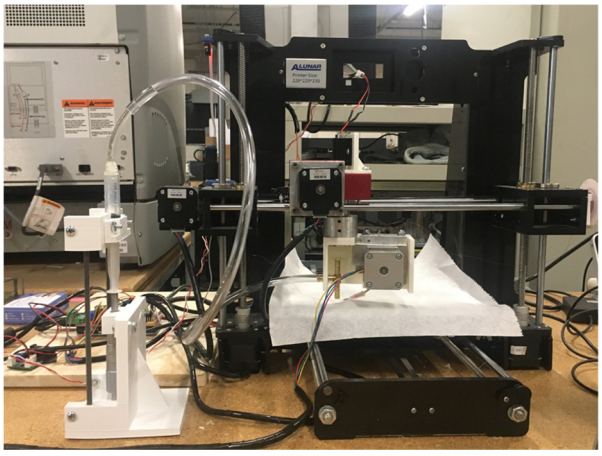

Fig. 6. The prototype system constructed for the VPP-based SMA wire bending process with the air bubble control and wire feeding systems.

discrete resin fixtures. The error analysis and the related improvement suggestions are presented at the end of this section.

7.1. Test cases using simple geometries

Fig. 7(a) and (b) show two bent wires using the VPP-based wire bending process to fabricate some basic shapes. The bending results verify the feasibility of the VPP-based wire bending process. The toolpaths of the laser and the wire extruder were computed from the CAD model of the input 2D shapes. The parameters used in the building process are presented as follows. The type of the liquid resin was a clear resin from Formlabs Inc. The feeding velocity of the wire was set at $v = 1$ mm/s. The laser power $P =$ 80 mW and the laser spot size was 500 μm. The curing depth $d = 1.5$ mm, and the width of the cured resin $w = 3.5$ mm.

In Fig. 7(a), 20 mm straight SMA wire was fed from a spool of wire and, consequently, fixed to a substrate by the photocured resin in the tank. In Fig. 7(b), the SMA wire was fixed by the solidified resin and bent into an input polygonal shape. The SMA wire was fixed on the substrate during the wire feeding and bending process so the bent wire cannot bounce back or change to other shapes even under the bending stress. The substrate in the experiments was a flat plastic platform that was black to reduce the light reflection. The photocured resin stuck firmly on the substrate and maintained the bent shape of the SMA wire.

7.2. Test cases using curves

To demonstrate the feasibility of using the VPP-based wire bending process to fabricate shapes with 2D curves, we designed and fabricated test cases using different letters. In Fig. 7(c), three wires were bent to form a “USC” pattern. The wire bending of the curves was generated by using multiple polygonal lines with small rotation angles. The feeding velocity, laser power, and curing depth were the same as the parameters used in the simple test cases. The printing results demonstrate the feasibility of bending a SMA wire into more complex shapes using the developed wire bending system. If the bottom substrate is a prefabricated 3D shape with a curved surface, the SMA wire can also be bent into a 3D shape that conforms to the substrate surface.

In addition, from the bending results, we can see the shape of the transparent resin fits well with the designed patterns. Although in the test results, the precision of the bent wire is relatively low, we believe the main reasons for the low precision of the bent wire are due to the inexpensive hardware components used in the prototype system, and the assembly errors especially the one between the laser and the rotary axis.

7.3. Discrete sealing fixtures in wire bending

By using the air bubble assisted separation process, the separation force of the immersed VPP tool is significantly reduced. However, the air-bubble-assisted separation makes the shape of the polymer fixtures difficult to control since the shape of the sealing resin is defined by the air bubble during the photocuring process. Fig. 7(d) shows the deformation of an air bubble during the laser nozzle movement. Consequently, the deformation of the air bubble will change the shape of the photocured resin, and we will not be able to fabricate polymer fixtures with consistent shapes and controllable thickness.

In order to achieve consistent sealing fixtures to secure the SMA wire on the substrate, we replaced the continuous fixturing, which was fabricated by keeping the laser constantly on, with the discrete

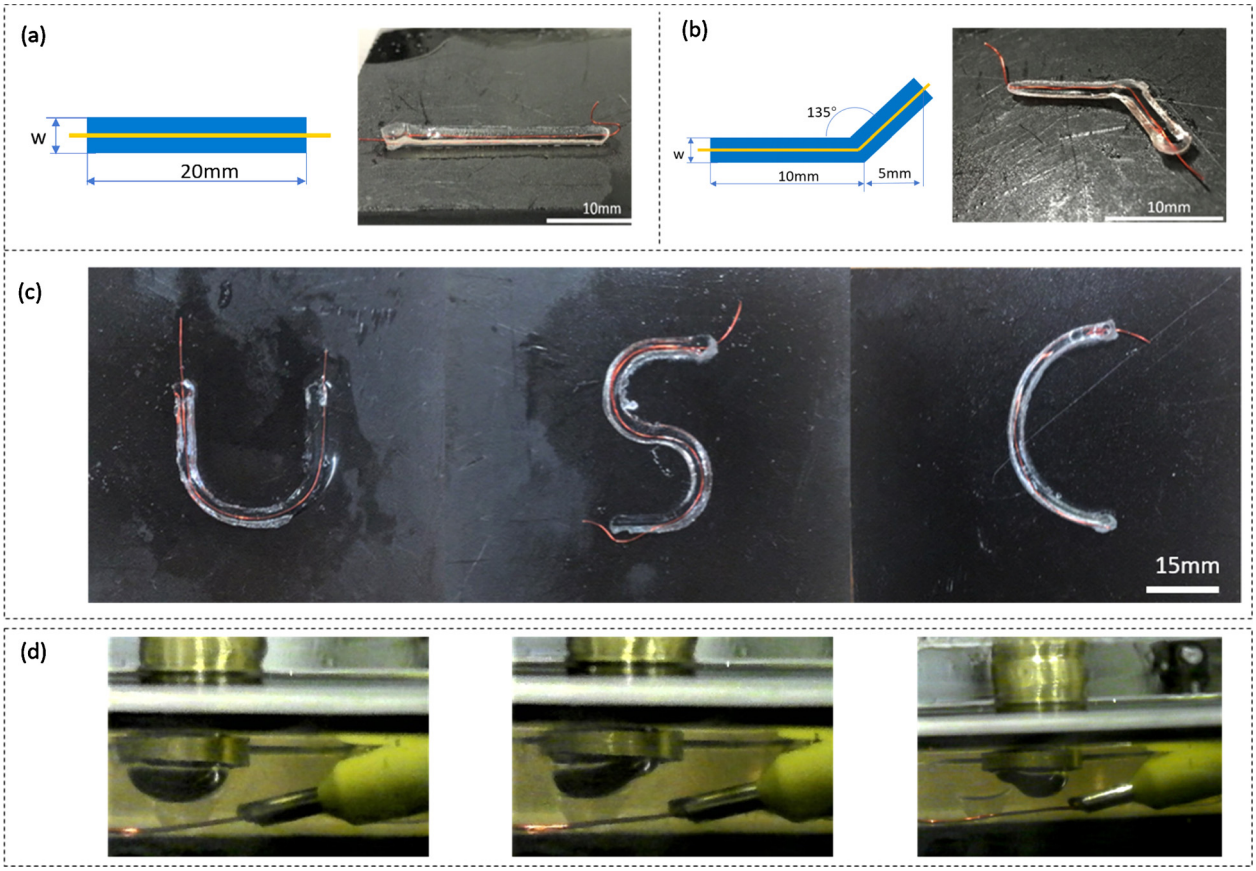

Fig. 7. Simple test cases. (a) Straight line test case; (b) polygonal line test case; (c) USC test case; and (d) bubble deformation during the printing process.

fixturing, which was fabricated by turning the laser on only when a stable air bubble has been formed with no laser nozzle movement. Hence, rather than fixed the wire by a continuous resin line, the SMA wire is now fixed by a set of discrete photocured dots. In the wire bending process, the laser cures the resin between the air bubble and the substrate while the SMA wire extruder is stopped with no movement. Then the laser will be turned off while the wire extruder is moving to the next position to cure another dot. Finally, the SMA wire will be sealed by a series of resin dots that can be planned by a fixture design software.

Tests of using air bubbles to photocure discrete dots were performed to study the shape of the fabricated polymer fixtures. The resin dots with three different intervals were shown in Fig. 8. Fig. 8(a–c) show the discrete resin dots with 2 mm, 3 mm, and 5 mm gaps, respectively, between the fixture dots. The identical and repeatable shapes of the sealing dots were fully defined by the bubble volume and the laser guide tube height. The use of the discrete resin dots as the SMA wire fixtures increases the robustness of the wire bending process. Fig. 8(d) shows a bent SMA wire using the discrete resin dots as the sealing and fixing method. Based on the result, we can see the SMA wire can be firmly fixed on the bottom substrate using a series of photocured resin dots that were designed based on a given wire pattern.

After the wire was bent into the desired shape on the substrate, the substrate was taken out and cleaned. Then the bent SMA was applied with 1.6 A current to reach over 500 °C, where the martensite structure transforms into austenite. Finally, after finishing the SMA wire training process, the fixing dots on SMA were removed using the aforementioned chemical solution. The bent SMA wire can accordingly memorize the trained shape. After distorting the SMA wire into an arbitrary shape, the trained SMA wire can recover its trained shape when the wire was put into hot water with 80 °C (refer to Fig. 8g).

7.4. Result analysis

We studied the precision of the VPP-based wire bending process by analyzing the shape difference between the bent SMA wire and the nominal CAD model. A total of 300 sample points on the bent wire before the SMA wire training were taken based on a photo of the wire. We then used the image processing technique to compare the sampling point positions on the bent wire with the nominal positions defined in the CAD model. The corresponding points were calculated in terms of their closest distance. The comparing result of the SMA wire before the SMA training process is shown in Fig. 8(e). The error distribution is shown in Fig. 8(f), which plots the errors in the bent wire in the sequence of the sample points along the SMA wire direction of letter 'U'. The average error of the bent SMA wire before training was 0.15 mm. The standard deviation of error was 0.0866 mm, and the maximum error was 0.44 mm.

The bent SMA wire was then trained by raising its temperature to over 500 °C to get the shape memory effect on the bent shape. After the training, the memorized shape was compared with the target CAD model. Fig. 8(g) shows the sample points of the SMA wire compared with the nominal CAD model after the wire was recovered from a deformed shape. The corresponding error distribution is shown in Fig. 8(h). The average error of the recovered SMA wire was 0.21 mm. The standard deviation of error was 0.114 mm and the maximum error was 0.64 mm. The analysis shows that the VPP-based SMA wire bending process has relatively high precision both before and after the SMA wire training process.

The recovery process of the SMA wire introduced additional errors to the wire bending result. Hence the average error increased as shown in Fig. 8(g). The error distribution figure shows that the maximum error occurs at the curved portion of the pattern. We believe one main reason is the tube used in the SMA wire extruder was around 800 μm in

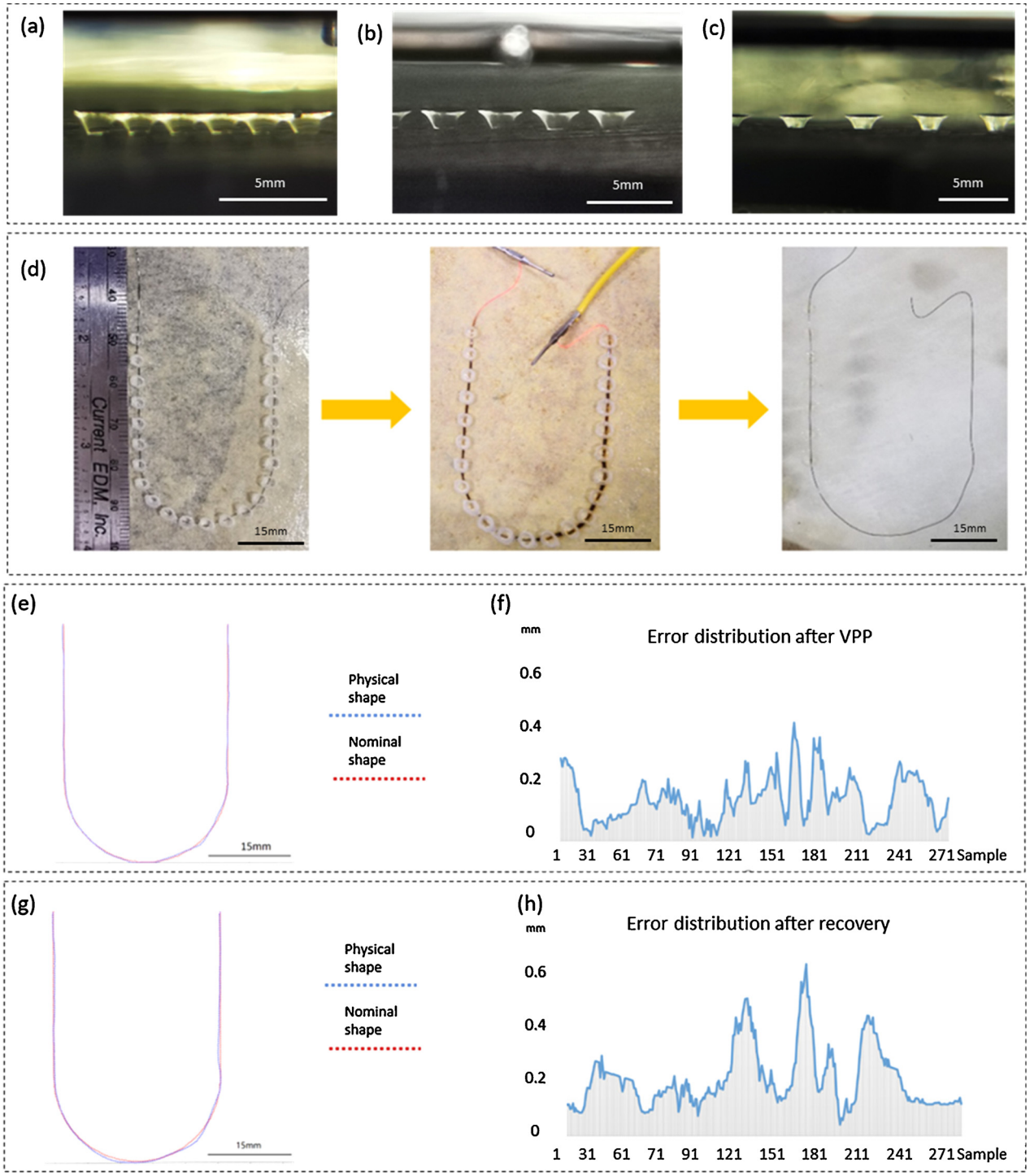

Fig. 8. A test case of letter 'U'. (a) The fixture using a set of polymer dots with 2 mm gap; (b) a set of polymer dots with 3 mm gap; (c) a set of polymer dots with 5 mm gap; (d) the U-shape test case; (e) the bent shape compared with the nominal shape before heat training; (f) the error distribution before heat training; (g) the recovered shape compared with the nominal shape after heat training and shape recovery in a raised temperature; and (h) the error distribution after heat training and shape recovery.

diameter, which is much larger than the bent SMA wire size of 150 μm. Hence it was difficult to accurately control the position of the SMA wire inside the extruding tube during the wire bending process. When the 150 μm SMA was extruded out from the wire extruder, the position of the SMA wire may have 650 μm variation. In the future, we plan to build a set of customized tubes with different sizes for a given SMA wire with a given diameter size. For example, for the 150 μm SMA wire, the tube's diameter size could be selected to be 200 μm. Consequently, the error at the curved portions will be significantly reduced. However, the tube needs to be replaced if SMA wires with different diameter sizes need to be bent.

7.5. Test case using complex shapes

A test case of two combined letters was performed to demonstrate the feasibility of using the VPP-based wire bender to fabricate more

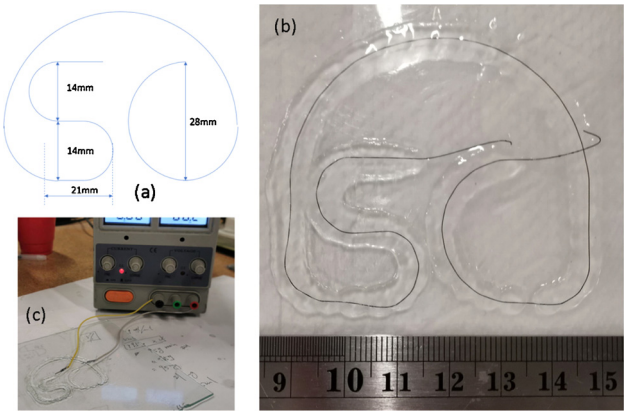

Fig. 9. A test case of a 'SC' pattern. (a) The CAD model of two combined letters; (b) the fabrication result; and (c) the training of the bent SMA wire.

complex shapes. In Fig. 9(a), the SMA wire was bent to form a "SC" pattern. The wire bending of the designed curve was performed using the developed SMA wire bending system. The feeding velocity, laser power, and curing depth were the same as the parameters used in the previous studies. The bent SMA wire is shown in Fig. 9(b). Finally, the high-temperature training of the bent wire on the substrate was performed (Fig. 9c). The test case further demonstrates the flexibility of bending a SMA wire into a more complex 2D shape using the VPP-based wire bending process.

8. Conclusion and future work

A new shape memory alloy wire bending process based on vat photopolymerization has been presented. A novel air bubble-assisted separation method was developed to reduce the detaching force of the photocured fixtures during the wire bending process. A prototype system that integrated both hardware and software systems has been developed. Various wire bending test cases were performed. The test results verified the feasibility of the VPP-based SMA wire bending process for various designed 2D shapes. The precision of the wire bending results has also been analyzed. The analysis results showed the VPP-based SMA wire bending process can achieve high precision for both before and after the SMA wire training process.

Some planned future work includes: (1) we will continue to increase the wire bending precision by improving the developed prototype system. Some main issues to be address include improving the assembly accuracy of the hardware components used in the prototype system and using a smaller extruder for given SMA wires; (2) we will test the building capability of the wire bending system on some 3D test cases based on customized substrates with curved surfaces; and (3) we will investigate potential applications enabled by the numerically controlled SMA wire bending system.

Acknowledgements

We acknowledge the funding support of theNational Science Foundation (NSF) CMMI 1151191 and USC's Daniel J. Epstein Institute.

References

[1] Ölander A. An electrochemical investigation of solid cadmium-gold alloys. AmChem Soc 1932;54:3819–33.
[2] Neugebauer R, Bucht A, Pagel K, Jung J. Numerical simulation of the activation behavior of thermal shape memory alloys. 2010. 76450J-J.
[3] Stoeckel D, Tinschert F. Temperature compensation with thermovariable rate springs in automatic transmissions. SAE technical paper series. SAE; 1991.
[4] Stoeckel D. Shape memory actuators for automotive applications. Mater Des 1990;11:302–7.
[5] Cleveland M.A. Apparatus and method for releasably joining elements. In: US Patent 7367738B2. The Boeing Co.; 2008.
[6] Huettl B, Willey C. Design and development of miniature mechanisms for small spacecraft. 14th AIAA/USU Small Satellite Conference, North Logan, UT, USA: Utah State University Research Foundation. 2000. p. 1–14.
[7] Carpenter B, Lyons J. EO-1 technology validation report. Lightweight flexible solar array experiment. 2001. NASA/GSFC Last updated: August, p. 8.
[8] Furuya Y, Shimada H. Shape memory actuators for robotic applications. Mater Des 1991;12:21–8.
[9] Sreekumar M, Nagarajan T, Singaperumal M, Zoppi M, Molfino R. Critical review of current trends in shape memory alloy actuators for intelligent robots. Ind Rob: Int J 2007;34:285–94.
[10] Furuya Y, Shimada H. Shape memory actuators for robotic applications. Mater Des 1991;12:21–8.
[11] Dahlgren J.M., Gelbart D. System for mechanical adjustment of medical implants. In: US Patent 2009/0076597A12009.
[12] Pfeifer R, Müller CW, Hurschler C, Kaierle S, Wesling V, Haferkamp H. Adaptable orthopedic shape memory implants. Procedia CIRP 2013;5:253–8.
[13] Wang Zhenlong, Hang Guanrong, Li Jian, Wang Yangwei, Xiao Kai. A micro-robot fish with embedded SMA wire actuated flexible biomimetic fin. Sens Actuators A Phys 2008;144:354–60.
[14] Kuribayashi Kaori, Tsuchiya Koichi. Self-deployable origami stent grafts as a biomedical application of Ni-rich TiNi shape memory alloy foil. Mater Sci Eng A 2006;419:131–7.
[15] Kuribayashi Katsutoshi. A new actuator of a joint mechanism using TiNi alloy wire. J Intell Mater Syst Struct 1986;4(4):47–58. Issue published: January 1.
[16] Tung AT, Park B-H, Liang DH, Niemeyer G. Laser-machined shape memory alloy sensors for position feedback in active catheters. Sens Actuators A Phys 2008;147:83–92.
[17] Gilbert Alfredo. An in-office iwre-bending robot for lingual orthodontics JCO/APRIL 2011.
[18] Rodrigue Hugo, Wei Wang, Bhandari Binayak. Fabrication of wrist-like SMA-based actuator by double smart soft composite casting. Smart Mater Struct 2015;24:125003.
[19] Mahmoudi M, Tapia G, Franco B, Ma J, Arroyave R, Karaman I, et al. On the printability and transformation behavior of nickel-titanium shape memory alloys fabricated using laser powder-bed fusion additive manufacturing. J Manuf Process 2018;35:672–80.
[20] Formlabs material library accessed on 02.26.2018.
[21] Wang Zhixin, Volinsky Alex A, Gallant Nathan D. Crosslinking effect on polydimethylsiloxane elastic modulus measured by custom-built compression instrument. Appl Polym 2020. https://doi.org/10.1002/app.41050.
[22] Jani Jaronie Mohd, Leary Martin, Subic Aleksandar. A review of shape memory alloy research, applications and opportunities. Mater Des 2014;56:1078–113.
[23] Chen Yong, Zhou Chi, Lao Jingyuan. A layerless additive manufacturing process based on CNC accumulation. Rapid Prototyp J 2011;17(3):218–27.
[24] Pan Yayue, Zhou Chi, Chen Yong, Partanen Jouni. Multi-tool and multi-axis CNC accumulation for fabricating conformal features on curved surfaces. J Manuf Sci Eng 2014;136(3).
[25] Mao Huachao, Zhou Chi, Chen Yong. LISA: linear immersed sweeping accumulation. J Manuf Process 2016;24:406–15.
[26] Li Xiangjia, Chen Yong. Micro-scale feature fabrication using immersed surface accumulation. J Manuf Process 2017;28:531–40.
[27] Pan Yayue, Chen Yong. Meniscus process optimization for smooth surface fabrication in stereolithography. Addit Manuf 2016;12:321–33.
[28] Flexinol® Actuator Wire Technical and Design Data.
[29] Wang ZG, Zu XT, Dai JY, Fu P, Feng XD. Effect of thermomechanical training temperature on the two-way shape memory effect of TiNi and TiNiCu shape memory alloys springs. Mater Lett 2003;57:1501–7.
[30] Xia Chunguang, Fang Nicholas. Fully three-dimensional microfabrication with a grayscale polymeric self-sacrificial structure. J Micromech Microeng 2009;19:115029. (7pp).